ISSN 1063-7761, Journal of Experimental and Theoretical Physics, 2018, Vol. 126, No. 4, pp. 485–496. © Pleiades Publishing, Inc., 2018.
Published in Russian in Zhurnal Eksperimental'noi i Teoreticheskoi Fiziki, 2018, Vol. 153, No. 4, pp. 582–596.

ORDER, DISORDER, AND PHASE TRANSITION IN CONDENSED SYSTEM

Electronic Structure of FeSe Monolayer Superconductors: Shallow Bands and Correlations[1]

I. A. Nekrasov[a,*], N. S. Pavlov[a,], and M. V. Sadovskii[a,b,***]**

[a] *Institute of Electrophysics, Ural Branch, Russian Academy of Sciences, Yekaterinburg, 620016 Russia*
[b] *Mikheev Institute of Metal Physics, Ural Branch, Russian Academy of Sciences, Yekaterinburg, 620290 Russia*
** e-mail: nekrasov@iep.uran.ru*
*** e-mail: pavlov@iep.uran.ru*
**** e-mail: sadovski@iep.uran.ru*

Received August 17, 2017

Abstract—Electronic spectra of typical single FeSe layer superconductor—FeSe monolayer film on $SrTiO_3$ substrate (FeSe/STO) obtained from ARPES data reveal several puzzles: what is the origin of shallow and the so called "replica" bands near the M-point and why the hole-like Fermi surfaces near the Γ-point are absent. Our extensive LDA+DMFT calculations show that correlation effects on Fe-3d states can almost quantitatively reproduce rather complicated band structure, which is observed in ARPES, in close vicinity of the Fermi level for FeSe/STO. Rather unusual shallow electron-like bands around the M-point in the Brillouin zone are well reproduced. Detailed analysis of the theoretical and experimental quasiparticle bands with respect to their origin and orbital composition is performed. It is shown that for FeSe/STO system the LDA calculated Fe-3d_{xy} band, renormalized by electronic correlations within DMFT gives the quasiparticle band almost exactly in the energy region of the experimentally observed "replica" quasiparticle band at the M-point. However, correlation effects alone are apparently insufficient to eliminate the hole-like Fermi surfaces around the Γ-point, which are not observed in most ARPES experiments. The Fermi surfaces remain here even if Coulomb and/or Hund interaction strengths are increased while overall agreement with ARPES worsens. Increase of number of electrons also does not lead to vanishing of this Fermi surface and makes agreement of LDA+DMFT results with ARPES data much worse. We also present some simple estimates of "forward scattering" electron-optical phonon interaction at FeSe/STO interface, showing that it is apparently irrelevant for the formation of "replica" band in this system and significant increase of superconducting T_c.

DOI: 10.1134/S1063776118040106

1. INTRODUCTION

The discovery of a class of iron pnictide superconductors has revived the intensive search and studies of new of high-temperature superconductors (cf. reviews [1–6]). Now there is general agreement that despite many similarities the nature of superconductivity in these materials significantly differs from that in high-T_c cuprates, and further studies of these new systems may lead to better understanding of the problem of high-temperature superconductivity in general.

Actually, the discovery of superconductivity in iron pnictides was very soon followed by its discovery in iron chalcogenide FeSe, which attracted much interest due to its relative simplicity, though its superconducting characteristics (under normal conditions) were rather modest ($T_c \sim 8$ K). Its electronic structure is now well understood and quite similar to that of iron pnictides (cf. review in [7]).

However, the general situation with iron chalcogenides has changed rather dramatically with the appearance of intercalated FeSe based systems raising the value of T_c to 30–40 K. It was soon recognized that their electronic structure is in general rather different form that in iron pnictides [8, 9]. The first system of this kind was $A_xFe_{2-y}Se_2$ (A = K, Rb, Cs) with $T_c \sim$ 30 K [10, 11]. It is generally believed that superconductivity in this system appears in an ideal 122-type structure, though most of the samples studied so far were multiphase, consisting of a mixture of mesoscopic superconducting and insulating (antiferromagnetic) structures (e.g. such as $K_2Fe_4Se_5$), complicating the studies of this system [12].

Further increase of T_c up to 45 K has been achieved by intercalation of FeSe layers with rather large molecules in compounds such as $Li_x(C_2H_8N_2)Fe_{2-y}Se_2$ [13] and $Li_x(NH_2)_y(NH_3)_{1-y}Fe_2Se_2$ [14]. The growth of T_c in these systems is sometimes associated with increase of the distance between the FeSe layers, i.e.

[1] The article was translated by the authors.

with the growth of the two-dimensional nature of the materials. Recently the active studies has started of $[Li_{1-x}Fe_xOH]FeSe$ system with the value of $T_c \sim 43$ K [15, 16], where a good enough single-phase samples and single crystals were obtained.

A significant breakthrough in the studies of iron chalcogenide superconductors occurred with the observation of a record high T_c in epitaxial films of single FeSe monolayer on $SrTiO_3$(STO) substrate [17]. These films were grown in [17] and in most of the papers to follow on the (001) plane of the STO. It should be noted that these films are very unstable on the air. Thus in many works the resistive transitions were mainly studied on films covered with amorphous Si or several FeTe layers, which significantly reduced the observed values of T_c. Unique measurements of the resistance of FeSe films on STO, done in [18] in situ, produced the record values of $T_c > 100$ K. However, up to now these results were not confirmed by independent measurements. Many ARPES measurements of the temperature behavior of superconducting gap in such films, now confidently demonstrate the values of T_c in the range of 65–75 K, sometimes even higher.

Films consisting of several FeSe layers usually produce the values of T_c much lower than those for the single-layer films [19]. Monolayer FeSe film on (110) plane of STO covered with several FeTe layers was studied in [20]. Resistivity measurements (including the measurements of the upper critical magnetic field H_{c2}) produced the value of $T_c \sim 30$ K. FeSe film, grown on $BaTiO_3$ (BTO) substrate, doped with Nb (with even larger values of the lattice constant ~3.99 Å), showed (in ARPES measurements) the value of $T_c \sim 70$ K [21]. In [22] quite high values of the superconducting gap were reported (from tunneling spectroscopy) for FeSe monolayers grown on (001) plane of TiO_2 (anatase), which in its turn was grown on the (001) plane of $SrTiO_3$. The lattice constant of anatase is actually very close to the lattice constant of bulk FeSe, so these FeSe film were essentially unstretched.

Single-layer FeSe films were also grown on the graphene substrate, but the value of T_c obtained was of the order of 8–10 K as in bulk FeSe [23]. This emphasizes the possible unique role of substrates such as $Sr(Ba)TiO_3$ in the significant increase of T_c.

More information on FeSe/STO films and other monolayer FeSe systems can be found in recent reviews [24, 25].

Electronic spectrum of iron pnictides is well understood now, both from theoretical calculations based on the modern band structure theory and ARPES experiments [1–6]. It is clear that almost all physics related to superconductivity is determined by electronic states of FeAs plane (layer). The spectrum of carriers in the vicinity of the Fermi level ±0.5 eV, where superconductivity is formed, practically have only Fe-3*d* character. The Fermi level is crossed by up to five bands (two or three hole and two electronic ones), forming a typical spectrum of a semi-metal.

In this rather narrow energy interval near the Fermi level these dispersions can be considered as parabolic [4, 26]. Most LDA+DMFT calculations [27, 28] show that the role of electronic correlations in iron pnictides, unlike in the cuprates, is relatively insignificant. It is reduced to more or less significant effective mass renormalization of the electron and hole dispersions, as well as to general narrowing ("compression") of the bandwidths.

The presence of the electron and hole Fermi surfaces of similar size, satisfying (approximately) the "nesting" condition plays an important role in the theories of superconducting pairing in iron arsenides based on (antiferromagnetic) spin fluctuation mechanism of pairing [4]. The electronic spectrum and Fermi surfaces in the Fe chalcogenides are very different from those in Fe pnictides. This raises the new problems for the understanding of microscopic mechanism of superconductivity in FeSe systems.

First LDA calculations of electronic structure of the $A_xFe_{2-y}Se_2$ (A = K, Cs) system were performed soon after its experimental discovery [29, 30]. Surprisingly enough, this spectrum was discovered to be qualitatively different from that of the bulk FeSe and spectra of practically all known systems based on FeAs.

Calculated Fermi surfaces for $K_xFe_{2-y}Se_2$ [29] differ significantly from the Fermi surfaces of FeAs systems—in the center of the Brillouin zone, there are only small Fermi sheets of electronic nature, while the electronic cylinders in the Brillouin zone corners are substantially larger. The shapes of the Fermi surfaces, typical for bulk FeSe and FeAs systems, can be obtained only at a much larger (apparently experimentally inaccessible) levels of the hole doping [29]. This shape of the Fermi surfaces in $K_xFe_{2-y}Se_2$ systems was almost immediately confirmed in ARPES experiments [31]. Note, that in this system it is clearly impossible to speak of any, even approximate, "nesting" properties of electron and hole Fermi surfaces.

LDA+DMFT and LDA' + DMFT calculations for $K_{1-x}Fe_{2-y}Se_2$ system for various doping levels were performed in [32–34]. The results of these calculations, in general, are in good qualitative agreement with the ARPES data [35, 36], which demonstrate strong damping of quasiparticles in the immediate vicinity of the Fermi level and a strong renormalization of the effective masses as compared to systems based on FeAs.

Below we compare the ARPES detected quasiparticle bands for the most interesting case of FeSe/STO with the results of our previous LDA+DMFT calculations for FeSe/STO and isolated FeSe layer [34], extended here to a wider range of model parameters, together with the analysis of the initial LDA calculated bands [37].

2. CRYSTAL STRUCTURE OF FeSe AND FeSe/STO SYSTEMS

Bulk FeSe system has probably the simplest crystal structure among iron high-T_c superconductors. It has tetragonal structure with the space group $P4/nmm$ and lattice parameters $a = 3.765$ Å, $c = 5.518$ Å. The experimentally observed crystallographic positions are: Fe ($2a$) (0.0, 0.0, 0.0), Se ($2c$) (0.0, 0.5, z_{Se}), $z_{Se} = 0.2343$ [38]. In our LDA calculations of isolated FeSe layer the slab technique was used with these crystallographic parameters.

The FeSe/STO crystal structure was taken from LDA calculation with crystal structure relaxation [39]. In slab approach FeSe monolayer was placed on three TiO_2–SrO layers to model the bulk $SrTiO_3$ substrate. The FeSe/STO slab crystal structure parameters used were a = 3.901 Å, Ti–Se distance 3.13 Å, Fe–O distance 4.43 Å, distance between top (bottom) Se ion and the Fe ions plane is 1.41 Å (1.3 Å). Atomic positions used were: Sr—(0.5 Å, 0.5 Å, –1.95 Å), O—(0.5 Å, 0, 0), (0, 0, –1.95 Å), Ti—(0, 0, 0).

The structure of the FeSe monolayer film on STO is shown in Fig. 1. Here the FeSe layer is directly adjacent to the surface TiO_2 layer of STO. The lattice constant within FeSe layer in a bulk samples is equal to 3.77 Å, while STO has substantially greater lattice constant equal to 3.905 Å, so that the single-layer FeSe film should be noticeably stretched, as compared with the bulk FeSe. However this tension quickly disappears as the number of subsequent layers grows.

3. COMPUTATION DETAILS

The electronic structures of isolated FeSe monolayer (imlFeSe) and FeSe monolayer on $SrTiO_3$ substrate were calculated within FP-LAPW method [40]. For considered systems projection on Wannier functions was done for Fe-3d and Se-4p states (imlFeSe) and for Fe-3d, Se-4p states and O-2p_y states of the topmost TiO_2 layer of $SrTiO_3$ substrate. To this end the standard wien2wannier interface [41] and wannier90 projecting technique [42] were applied.

The DMFT(CT-QMC) [43–46] computations were done at reciprocal temperature $\beta = 40$ eV^{-1} (~290 K) with about 10^8 Monte-Carlo sweeps. In this work we considered a range of interaction parameters of the Hubbard model around typical values of U = 5.0 eV and $J = 0.9$ eV for isolated FeSe and FeSe/STO and several doping levels 0.1, 0.2, and 0.3 electrons per Fe ion, thus extending the results of our previous work [34].

We used the self-consistent fully-localized limit definition of the double-counting correction [47] was used. Thus computed values of Fe-3d occupancies and corresponding double-counting energies are E_{dc} = 31.63 eV, $n_d = 7.35$ (imlFeSe), $E_{dc} = 30.77$ eV, $n_d = 7.16$ (FeSe/STO).

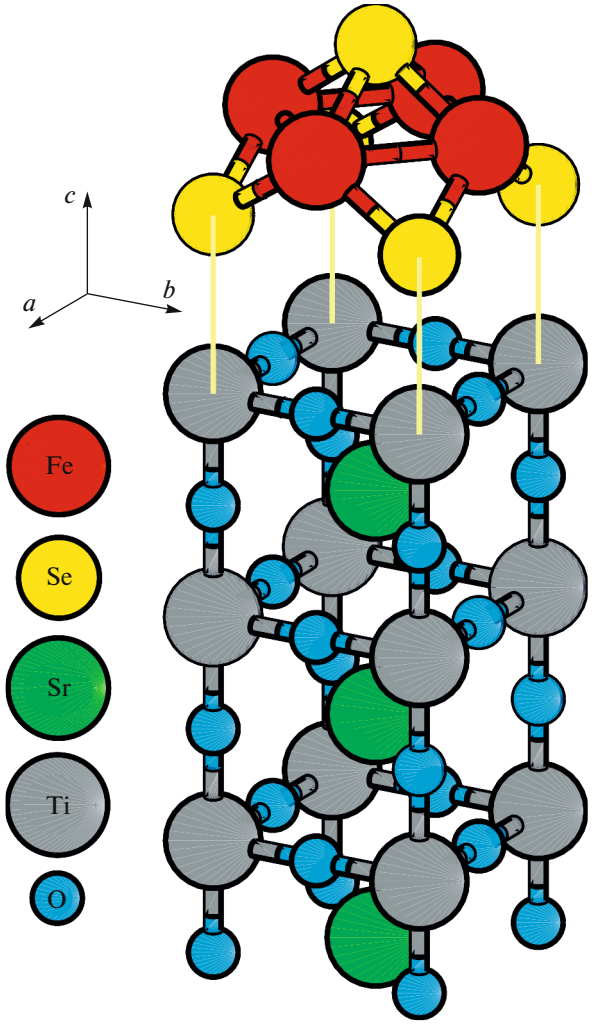

Fig. 1. (Color online) Crystal structure of FeSe monolayer on (001) surface of $SrTiO_3$ with TiO_2 topmost layer.

The LDA+DMFT spectral function maps were obtained after analytic continuation of the local self-energy $\Sigma(\omega)$ from Matsubara to real frequencies. To this end we have used the Pade approximant algorithm [48] and checked the results with the maximum entropy method [49] for the Green's function.

4. RESULTS AND DISCUSSION

It turns out that in FeSe layered systems correlation effects are quite important, leading to a noticeable change of LDA calculated dispersions. In contrast to iron arsenides, where the quasiparticle bands near the Fermi level are well defined, in the $K_{1-x}Fe_{2-y}Se_2$ compounds in the vicinity of the Fermi level we observe much stronger suppression of the intensity of quasiparticle bands [32–34]. This reflects the stronger role of correlations in this system, as compared to iron arsenides. The value of the quasiparticle renormalization (correlation narrowing) of the bands at the Fermi

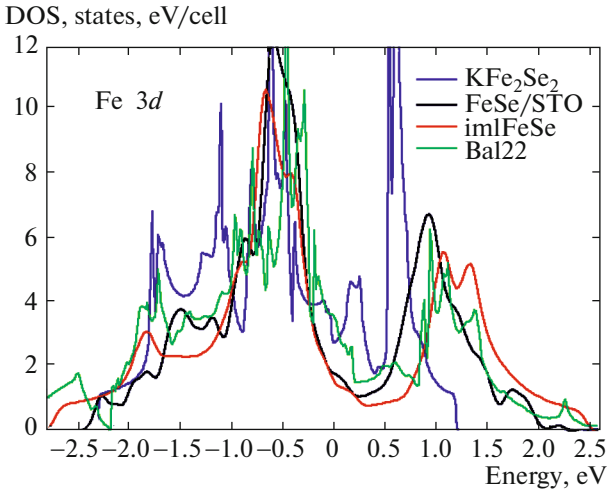

Fig. 2. (Color online) LDA calculated densities of states (DOS) for various iron-based superconductors: imlFeSe (red, $W = 5.2$ eV), Ba122 (green, $W = 4.8$ eV), FeSe/STO (black, $W = 4.3$ eV), KFe_2Se_2 (blue, $W = 3.5$ eV) Fermi level is at zero energy.

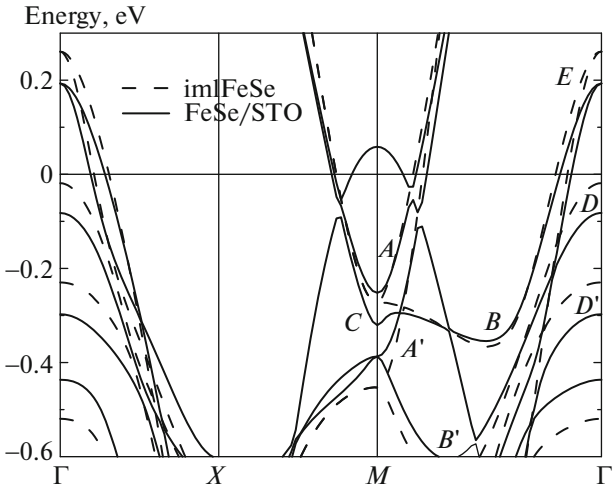

Fig. 3. LDA band dispersions of paramagnetic isolated FeSe monolayer (dashed curve) and paramagnetic FeSe/STO (solid curve). The letters designate bands in the same way as in Fig. 4. The Fermi level E_F is at zero energy.

level is 4–5, whereas in iron arsenides this factor is only 2–3 for the same values of the interaction parameters. That can be understood in terms of W—width of bare LDA Fe-3d states. As it is shown on Fig. 2 the largest bandwidth $W = 5.2$ eV has isolated FeSe monolayer (red curve), then comes Ba122 (green curve) with $W = 4.8$ eV, FeSe/STO (black curve) with $W = 4.3$ eV and finally the most narrow bare band has KFe_2Se_2 system (blue curve)—$W = 3.5$ eV. In its turn such lowering of the W can be explained by the growth of lattice constant from imlFeSe to KFe_2Se_2.

4.1. DFT/LDA Results

For further detailed analysis of our LDA+DMFT data let us start from the results of our LDA calculations [37] of the spectrum for the isolated FeSe monolayer together with FeSe layer on STO substrate are shown in Fig. 3. This spectrum has the form typical for FeAs based systems and bulk FeSe as discussed in detail above. However ARPES experiments [50–52] are in striking disagreement with these results. Actually, in FeSe monolayers on STO only electron-like Fermi surface sheets are observed around the M-points of the Brillouin zone, while hole-like sheets, centered around the Γ-point (in the center of the zone), are just absent [50]. Similarly to intercalated FeSe systems there is no place for "nesting" of Fermi surfaces—there are just no surfaces to "nest"!

In order to explain this contradiction between ARPES experiments [50] and band structure calculations reflected in the absence of hole-like cylinders at the Γ-point, one can suppose it to be the consequence of FeSe/STO monolayer stretching due to mismatch of lattice constants of the bulk FeSe and STO. We have studied this problem by varying the lattice parameter a and Se height z_{Se} in the range ±5% around the bulk FeSe parameters with the account of lattice relaxation. The conclusion was that the changes of lattice parameters do not lead to qualitative changes of FeSe Fermi surfaces and the hole-cylinders in the Γ-point always remain more or less intact.

However, there is another rather simple possible explanation for the absence of hole-like cylinders and the observed Fermi surfaces can be obtained assuming that the system is doped by electrons. The Fermi level has to be moved upwards in energy by the value of ~0.2–0.25 eV, corresponding to the doping level of 0.15–0.2 electron per Fe ion (see Fig. 3).

The nature of this doping, strictly speaking, is not fully understood. There is a common belief that it is associated with the formation of oxygen vacancies in the $SrTiO_3$ substrate (in the topmost layer of TiO_2), occurring during the various technological steps used during film preparation, such as annealing, etching, etc. It should be noted that the formation of the electron gas at the interface with the $SrTiO_3$ is rather widely known phenomenon, which was studied for a long time [53]. At the same time, for FeSe/STO system this issue was not analyzed in detail and remains unexplained (see, however, recent [54, 55].

4.2. LDA+DMFT Results

Let us consider now in detail the results of our LDA+DMFT calculations, extending the discussion presented in [34].

In Fig. 4 we present the summary of our calculation results (shown on panels (a), (d), (e), (h)), compared

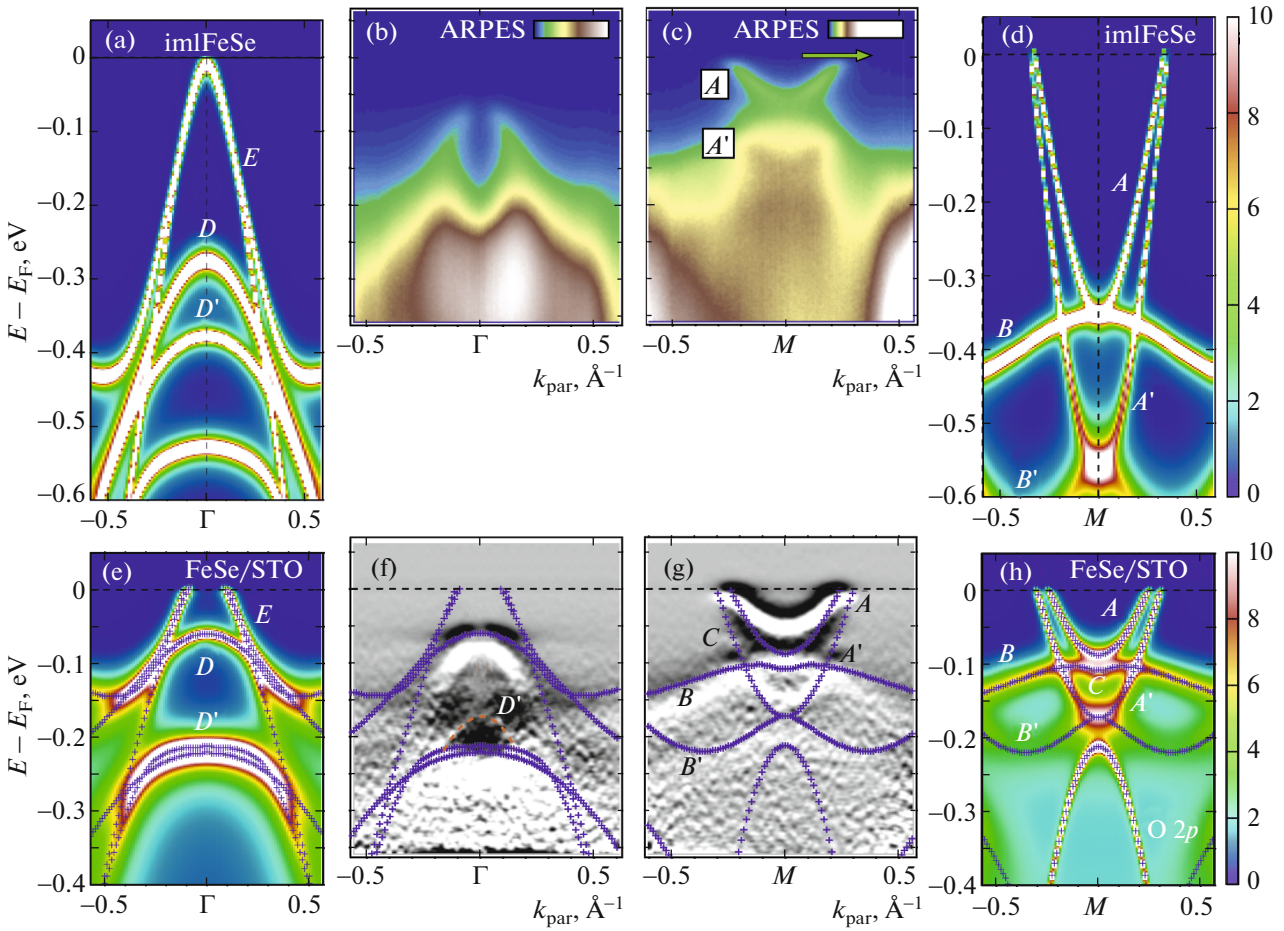

Fig. 4. (Color online) (a, d) LDA+DMFT spectral function maps of isolated FeSe monolayer [34]; (b, c) experimental ARPES data around Γ and *M* points, and (f, g) corresponding second derivatives of ARPES data for FeSe/STO [56] with LDA+DMFT spectral function maxima shown with crosses; (e, h) LDA+DMFT spectral function maps [34] with maxima shown with crosses for FeSe/STO. To mark similar features of experimental and theoretical spectral function maps *A*, *B*, *C*, *D*, *E* letters are used (the same as in Fig. 3 for LDA bands). Fermi level is at zero energy.

with experimental ARPES data [56], shown on panels (b), (c), (f), (g). LDA+DMFT spectral function maps of isolated FeSe monolayer under electron doping 0.3*e*/FeSe are shown in Figs. 4a and 4d at Γ and *M* points respectively. For FeSe/STO LDA+DMFT under doping 0.2*e*/FeSe, the calculated spectral function maps are shown on (e), (h) panels at Γ and *M* points. For detailed comparison with ARPES data in Figs. 4e, 4f, 4g, 4h we also plot (by crossed) the dispersions of our calculated maxima of the spectral density. The obtained LDA bandwidth *W* of Fe-3*d* band in isolated FeSe monolayer it is 5.2 eV, which is much larger than 4.3 eV obtained for FeSe/STO. This is due to the lattice constant a expanded from $a = 3.765$ Å to $a = 3.901$ Å in going from isolated FeSe monolayer to FeSe/STO (see also Fig. 2). Thus for the same interaction strength and doping levels LDA+DMFT calculations demonstrate substantially different band narrowing due to correlation effects. It is a factor of 1.5 in isolated FeSe monolayer (same as bulk FeSe) and a factor of 3 in FeSe/STO. Thus, we may conclude that FeSe/STO system is more correlated as compared with the bulk FeSe or isolated FeSe layer with respect to U/W ratio.

Most of features observed in the ARPES experiments (Figs. 4f, 4g) can be identified with our calculated LDA+DMFT spectral function maps (Figs. 4e, 4h). The experimental quasiparticle bands around *M*-point marked by *A*, *B*, and *C* (Figs. 4g, 4h) correspond mainly to Fe-3d_{xz} and Fe-3d_{yz} states (Fig. 5a), while the *A*' and *B*' quasiparticle bands have predominantly Fe-3d_{xy} character (Fig. 5b).

The *C* quasiparticle band near *M*-point appeared due to lifting of degeneracy of Fe-3d_{xz} and Fe-3d_{yz} bands (see Fig. 4h) (which is in contrast to isolated FeSe layer, see Fig. 4d). The origin of this band splitting is directly related to the z_{Se} height difference below and above Fe ions plane due to the presence of interface with $SrTiO_3$.

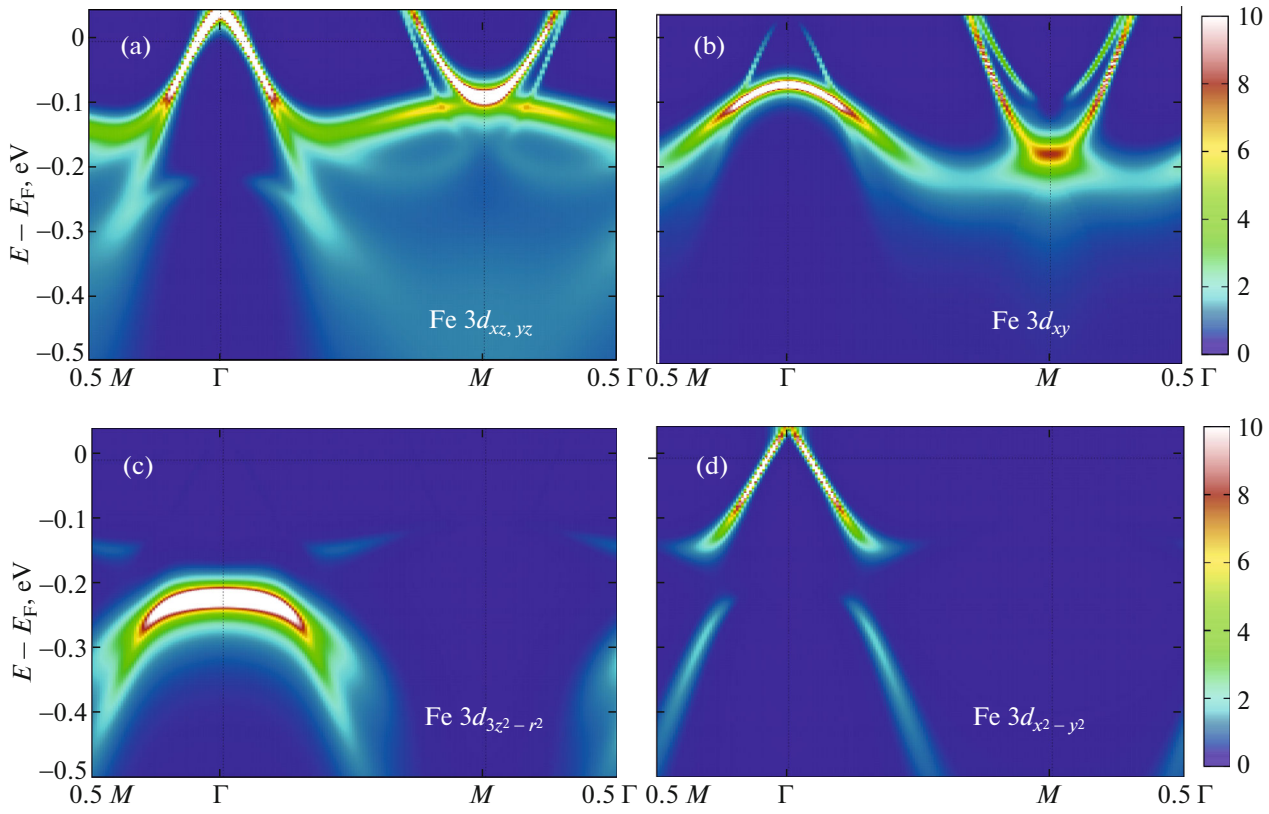

Fig. 5. (Color online) LDA+DMFT spectral function maps for different Fe-3*d* orbitals of FeSe monolayer on $SrTiO_3$ substrate: (a) Fe-3d_{xz} and Fe-3d_{yz}, (b) Fe-3d_{xy}, (c) Fe-3$d_{3z^2-r^2}$, (d) Fe-3$d_{x^2-y^2}$. Fermi level is at zero energy.

Actually, all quasiparticle bands in the vicinity of *M*-point can be well represented as LDA bands compressed by a factor of 3 due to electronic correlations. This fact is clearly supported by our calculated LDA band structure shown on Fig. 3, where different bands are marked by letters identical to those used in Fig. 4.

Near the *M*-point we also observe the O-2p_y band (in the energy interval below −0.2 eV (Fig. 4h) originating from TiO_2 layer adjacent to FeSe. Due to doping level used this O-2p_y band goes below the Fermi level in contrast to LDA picture shown in Fig. 3 where O-2p_y band crosses the Fermi level and forms hole pocket. This observation rules out possible nesting effects between these bands which might be expected from LDA results [37].

The appearance of *A*' (and in some works *B*') band in FeSe/STO is usually attributed to forward scattering interaction with 100 meV optical phonon of STO substrate [56–60]. Below in Section 5 we will provide some estimates of such electron-optical phonon coupling strength which in fact is obtained to be exponentially small for the case of FeSe/STO making this scenario of the "replica" band formation rather improbable. Our calculations clearly show that *A*' band of purely electronic nature appears almost exactly at the energies of the so called "replica" band with no reference to phonons. Quasiparticle masses (as listed in Table 1) of *A* and *A*' bands differ from each other not more then by 10%. If we concentrate our attention close to *M*-point the shapes of *A* and *A*' bands are almost the same within the accuracy of experimental data. Let us note here that equal shapes (or the same quasiparticle masses) of *A* and *A*' bands is a keypoint of phenomenological "replica" band description in [56, 59]. One should say here that the *B*' band is well seen in our LDA+DMFT results (Figs. 4g, 4h) also without introducing of any electron-phonon coupling. In contrast to $K_{0.76}Fe_{1.72}Se_2$ case [34] in FeSe/STO system the *A*' band is well detected in the ARPES near *M*-point while near Fermi level it is strongly suppressed. This may be due to some matrix elements effects as discussed in [61, 62] and references therein, as well as in [28, 61] in the context of NaFeAs compound. Again, similar to the $K_{0.76}Fe_{1.72}Se_2$ case we propose that *A*' and *B*' bands are common feature of FeSe-based materials and should be experimentally observed irrespective of the electron-phonon scenario of the "replica" band.

Thus, for FeSe/STO system we observe the general agreement between the results of LDA+DMFT calculations of [34] (Fig. 4h) and ARPES data [56] (Fig. 4g) on semi-quantitative level with respect to relative posi-

tions of quasiparticle bands. Note that the Fermi surfaces, which can be extracted from our LDA+DMFT calculations, formed by the A and A' bands are nearly the same as the Fermi surface observed at M-point by ARPES.

Now let us discuss the bands around the Γ-point, which are shown on panels (a), (b), (e), (f) of Fig. 4. Here the situation is somehow much simpler than in the case of M-point. One can see here only two bands observed in the experiment (Fig. 4f). The D quasiparticle band has predominantly Fe-3d_{xy} character (see Fig. 5a), while the D' quasiparticle band originates from Fe-3$d_{3z^2-r^2}$ states (see Fig. 5c). The relative locations of LDA+DMFT calculated D and D' bands are quite similar to the ARPES data.

Main discrepancy of LDA+DMFT results and ARPES data here is the E band shown in Fig. 4e which is not observed in the ARPES. This band corresponds to a hybridized band of Fe-3d_{xz}, Fe-3d_{yz} and Fe-3d_{xy} states (see Fig. 5). In principle some traces of this band can be guessed in the experimental data of Fig. 4f around –0.17 eV and near the **k**-point (0.5 Å). Surprisingly these are missed in the discussion of [56]. Actually, the ARPES signal from E band can be weakened because of the Fe-3d_{xy} contribution [28, 61, 62] and thus might be indistinguishable from D band.

Trying to achieve the better agreement with experiments we have also examined the reasonable increase of Coulomb interaction parameters within LDA+DMFT and some different doping levels.

In Fig. 6 we present doping dependence of the LDA+DMFT spectral function map of FeSe monolayer on $SrTiO_3$ substrate (FeSe/STO) for U = 5 eV and J = 0.9 eV. We assumed here three doping levels: +0.1, +0.2, and +0.3 per Fe ion. In general such electron doping leads to a more or less rigid band shift. However with electron doping growth the correlation strength decreases as can be seen in the upper part of the Table 1. Especially correlations are nearly twice weaker for t_{2g} orbitals. It is rather well known behavior for iron-based superconductors [63]. One should note here that the doping level of +0.3e leads to almost vanishing Fermi surface at the Γ-point (see the top of the right column of the Fig. 6) as it is observed in the ARPES. However, at this doping the general agreement between LDA+DMFT and ARPES bands is much worser than in the case of +0.2e doping discussed above.

The Coulomb interaction dependence of the LDA+DMFT spectral function maps of FeSe/STO is shown on Fig. 7, where we present our results for U = 4.0, 5.0, and 6.0 eV. As expected the increase of U leads to stronger correlation effect (see middle part of the Table 1). The growth of U leads to more or less uniform bands compression. The best agreement with ARPES detected bands is found for U = 5 eV. Thus, we can see that the increase of U does not lead to vanishing hole Fermi surface near the Γ-point.

Table 1. LDA+DMFT obtained mass renormalization values for FeSe/STO system for various model parameters U, J and n for different Fe-3d orbitals

	$d_{x^2-y^2}$	d_{yz}	$d_{3z^2-r^2}$	d_{xz}	d_{xy}
U = 5.0 eV, J = 0.9 eV (fixed)					
+0.1e/FeSe	2.47	4.25	2.36	4.04	4.32
+0.2e/FeSe	2.03	3.07	2.04	2.93	3.12
+0.3e/FeSe	1.84	2.42	1.83	2.33	2.47
+0.2e/FeSe, J = 0.9 eV (fixed)					
U = 4.0 eV	1.71	2.29	1.74	2.21	2.34
U = 5.0 eV	2.03	3.07	2.04	2.93	3.12
U = 6.0 eV	2.74	5.11	2.57	4.84	5.14
+0.2e/FeSe, U = 5.0 eV (fixed)					
J = 0.7 eV	1.49	1.73	1.56	1.69	1.75
J = 0.8 eV	1.63	2.05	1.70	1.99	2.08
J = 0.9 eV	2.03	3.07	2.04	2.93	3.12

Perhaps the most drastic effect on the spectrum of FeSe/STO can be achieved changing of the Hund's coupling value J. In some sense it is clear from the very beginning since iron-based superconductors, according to the common belief, are the so called "Hund's metals" [64]. In Fig. 7 we show Hund's coupling dependence of the LDA+DMFT spectral function map for J = 0.7, 0.8, and 0.9 eV. In the case of J growth, the quasiparticle bands compression is more evident in comparison with the case of increasing U (Fig. 8). Mass renormalization changes approximately by a factor of 2 (see lower part of the Table 1) similar to those of U or n variation.

Finally, one can say that rather moderate change of model parameters for the FeSe/STO system can produce rather significant change of its electronic structure, so that the experimentally observed spectrum may result from rather fine tuning of these parameters.

5. "REPLICA" BAND AND ELECTRON–OPTICAL PHONON COUPLING IN FeSe/STO

As we mentioned earlier, the most popular explanation of the appearance of the "replica" band around the M-point in FeSe/STO is related to FeSe electrons interaction with ~100 meV optical phonons in STO. This idea was first proposed in [56], where this band was experimentally observed for the first time. In this work (see also [65]) it was also shown that due to the peculiar nature of electron–optical phonon interactions at FeSe/STO interface, the appropriate coupling constant is exponentially suppressed with transferred momentum and can be written as

$$g(\mathbf{q}) = g_0 \exp(-|\mathbf{q}|/q_0), \quad (1)$$

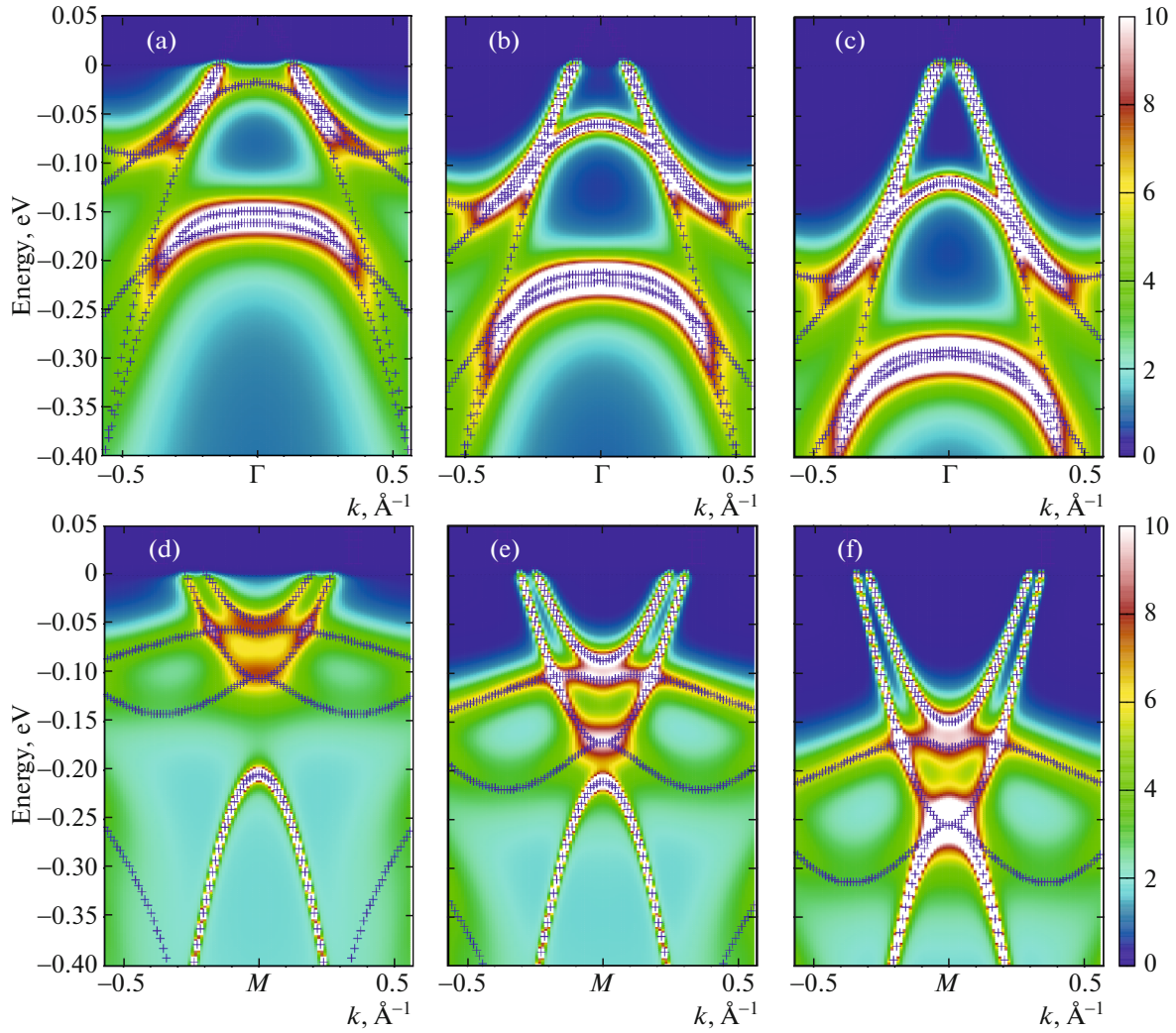

Fig. 6. (Color online) LDA+DMFT spectral function map of FeSe/STO for different electron doping levels (per Fe ion) for $U =$ 5.0 eV and $J = 0.9$ eV: $+0.1e$, $+0.2e$, $+0.3e$ (from left to right) near Γ (upper line) and M high symmetry points (lower line). Fermi level is at zero energy.

where typically $q_0 \sim 0.1\frac{\pi}{a} \ll p_F$ (a is the lattice constant and p_F is the Fermi momentum), leading to the picture of nearly forward scattering of electrons by optical phonons. This picture was further developed in model approach of [59, 60] where it was shown, that such coupling can also lead to rather significant increase of the temperature of superconducting transition T_c in accordance with earlier ideas developed by Dolgov and Kulić [66, 67] (see also the review in [25]). However, the significant effect here can be achieved only for the case of large enough effective coupling of electrons with such forward scattering phonons.

The standard dimensionless electron-phonon coupling constant of Eliashberg theory for the case of optical (Einstein) phonon at FeSe/STO interface can be written as (N is the number of lattice sites) [68]:

$$\lambda = \frac{2}{N\Omega_0}\frac{\sum_{\mathbf{p},\mathbf{q}}|g(\mathbf{q})|^2\delta(\epsilon(\mathbf{p})-\mu)\delta(\epsilon(\mathbf{p}+\mathbf{q}))-\mu-\Omega_0)}{\sum_{\mathbf{p}}\delta(\epsilon(\mathbf{p})-\mu)}, \quad (2)$$

where we explicitly introduced (optical) phonon frequency Ω_0 in δ-function, which is usually neglected in adiabatic approximation. In FeSe/STO system we actually have $\Omega_0 > E_F$, so that it is obviously should be kept finite.

For simple estimates we can assume the linearized spectrum of electrons (v_F is Fermi velocity): $\xi_p \equiv \epsilon(\mathbf{p}) - \mu \approx v_F(|\mathbf{p}| - p_F)$ so that all calculations can be done explicitly in analytic form. Now using (1) in (2) for two-dimensional case we can write:

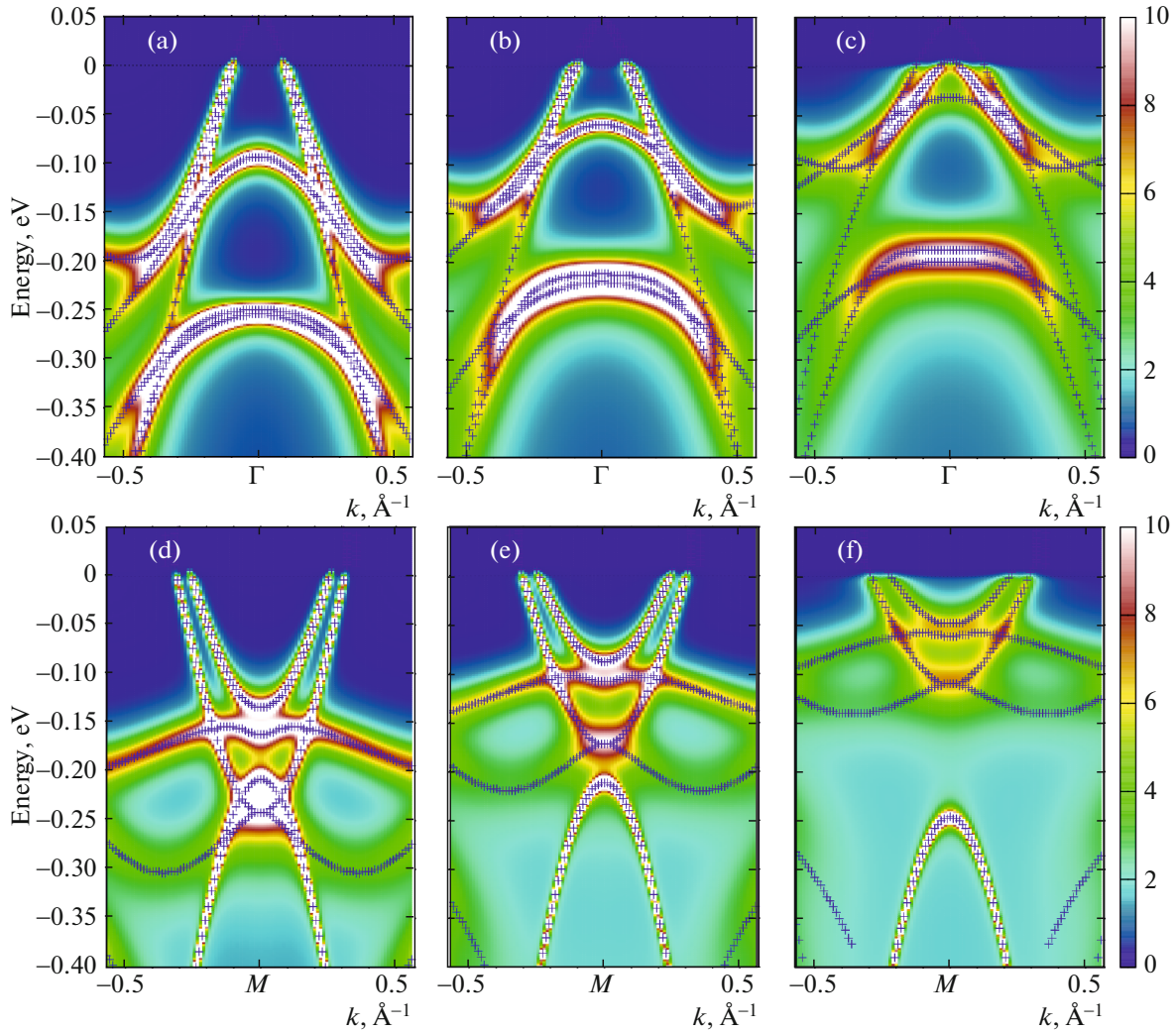

Fig. 7. (Color online) LDA+DMFT spectral function map of FeSe/STO for different values of U for $n = +0.2e$ and $J = 0.9$ eV: 4, 5, and 6 eV (from left to right) near Γ (upper line) and M high symmetry points (lower line). Fermi level is at zero energy.

$$\lambda = \frac{2}{\Omega_0} g_0^2 \int_{-\infty}^{\infty} d\xi_p \delta(\xi_p) \int \frac{d^2q}{(2\pi)^2} \exp\left(-\frac{2q}{q_0}\right) \times \delta(\xi_p - \Omega_0 + v_F q \cos\phi) = \frac{2g_0^2}{\Omega_0} \frac{a^2}{4\pi^2} \times \int_0^{\infty} dq q \exp\left(-\frac{2q}{q_0}\right) \int_0^{2\pi} d\phi \delta(v_F q \cos\phi - \Omega_0). \quad (3)$$

Then, after the direct calculation of all integrals, we obtain:

$$\lambda = \frac{g_0^2 a^2}{\pi^2 v_F^2} K_1\left(\frac{2\Omega_0}{v_F q_0}\right), \quad (4)$$

where $K_1(x)$ is Bessel function of imaginary argument (McDonald function). Using the well known asymptotic behavior of $K_1(x)$ and dropping some irrelevant constants we get:

$$\lambda \sim \lambda_0 \frac{q_0}{4\pi p_F}, \quad (5)$$

for $\frac{\Omega_0}{v_F q_0} \ll 1$, and

$$\lambda \sim \lambda_0 \frac{\Omega_F}{\pi \varepsilon_F} \sqrt{\frac{v_F q_0}{\Omega_0}} \exp\left(-\frac{2\Omega_0}{v_F q_0}\right), \quad (6)$$

for $\frac{\Omega_0}{v_F q_0} \gg 1$. Here we introduced the standard dimensionless electron–phonon coupling constant as:

$$\lambda_0 = \frac{2g_0^2}{\Omega_0} N(0), \quad (7)$$

where $N(0)$ is the density of states at the Fermi level per one spin projection.

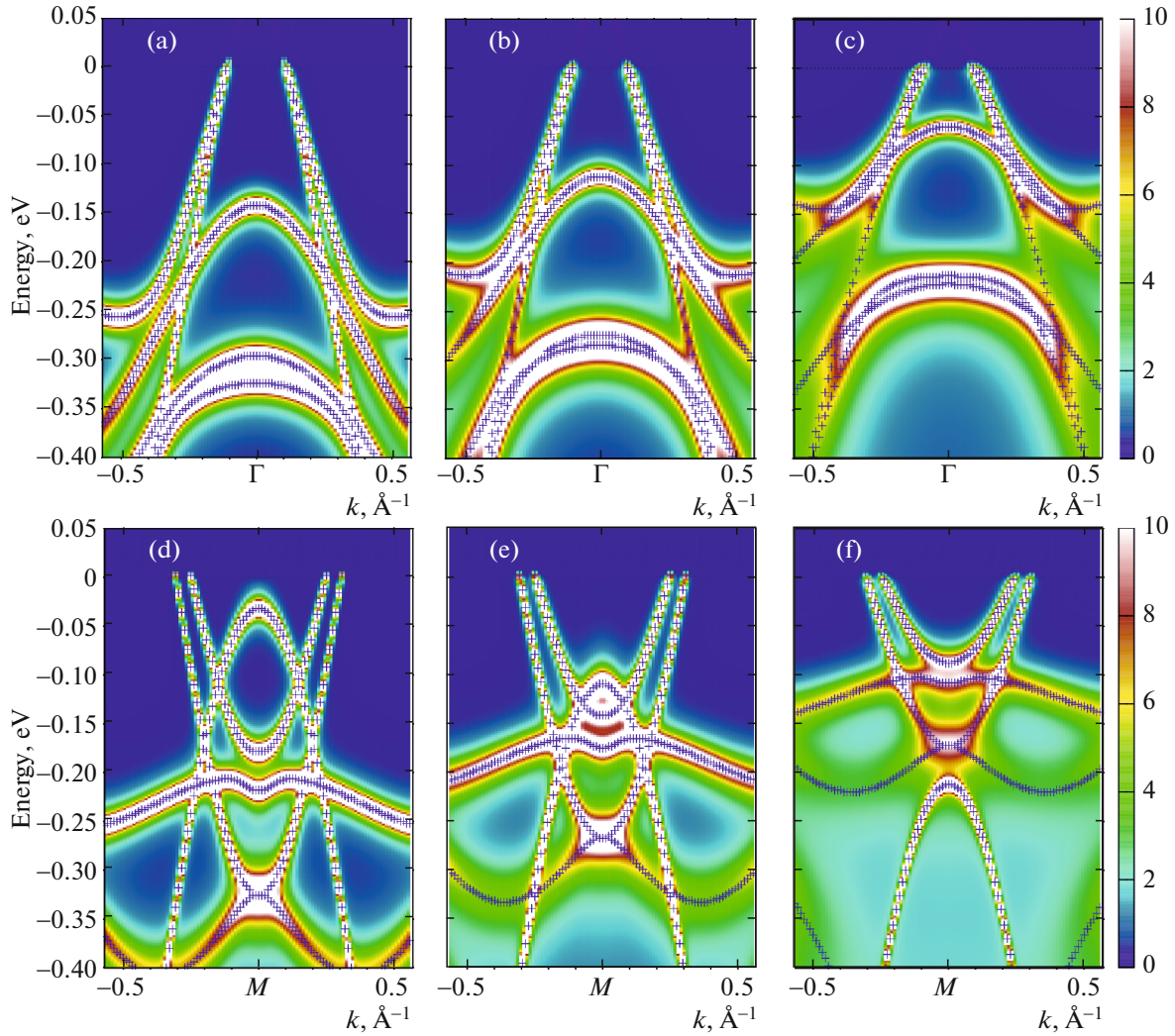

Fig. 8. (Color online) LDA+DMFT spectral function map of FeSe/STO for different values of J for $n = +0.2e$ and $U = 5$ eV: 0.7, 0.8, and 0.9 eV (from left to right) near Γ (upper line) and M high symmetry points (lower line). Fermi level is at zero energy.

Now it becomes obvious that the pairing constant is exponentially suppressed for $\frac{\Omega_0}{v_F q_0} > 1$, which is typical for FeSe/STO interface, where $\Omega_0 > E_F \gg v_F q_0$ [25], making the appearance of the "replica" band and T_c enhancement due to coupling of FeSe electrons with optical phonons of STO quite improbable. Similar conclusions were reached from first principles calculations of [69] and the analysis of screening of electron-phonon interactions at FeSe/STO interface in [70].

As we have seen above, our LDA+DMFT calculations of FeSe/STO system produced entirely different explanation for the origin of the "replica" band not related to electron-phonon interactions.

6. CONCLUSIONS

Our extended LDA+DMFT results for FeSe monolayer material—FeSe/STO provide the scenario of formation of puzzling shallow bands at the M-point due to correlation effects on Fe-3d states only. The detailed analysis of ARPES detected quasiparticle bands and LDA+DMFT results shows that the closer to the Fermi level shallow band (at about 50 meV) is formed by the degenerate Fe-3d_{xz} and Fe-3d_z bands renormalized by correlations. Moreover, second shallow band (at about 150 meV) can be reasonably understood as simply correlation renormalized LDA Fe-3d_{xy} band and appears almost at the same energies as the so called "replica" band observed in ARPES for FeSe/STO, usually attributed to electron interactions with optical phonons of STO. The influence of STO substrate is reduced only to the removal of degeneracy

of Fe-3d_{xz} and Fe-3d_{yz} bands in the vicinity of M-point. Thus we conclude that such rather unusual band structure near Fermi level with several electron-like shallow bands is a common feature of FeSe monolayer materials and possibly can be fully resolved in future ARPES experiments.

Our estimates of electron–optical phonon coupling strength show that it is exponentially small for the case of FeSe/STO parameters, so that the common interpretation of the "replica" band as due this interaction seems to be rather unrealistic.

Correlation effects alone are apparently unable to eliminate completely the hole-like Fermi surface at the Γ-point, which is not observed in most ARPES experiments on FeSe/STO system. At the same time, for the most of the calculated bands close to the Γ-point the agreement with ARPES experiments is rather satisfactory.

It was also shown that the increase of electron doping and/or Coulomb interaction does not improve the overall agreement of our calculations with ARPES data.

ACKNOWLEDGMENTS

This work was done under the State contract (FASO) no. 0389-2014-0001 and supported in part by Russian Foundation for Basic Research (project no. 17-02-00015) and the Program of Fundamental Research of the Presidium of the Russian Academy of Sciences "Fundamental problems of high-temperature superconductivity." NSP work was also supported by the President of Russia, grant for young scientists no. MK-5957.2016.2. The CT-QMC computations were performed at "URAN" supercomputer of the Institute of Mathematics and Mechanics of the Ural Branch, Russian Academy of Sciences.

REFERENCES

1. M. V. Sadovskii, Phys. Usp. **51**, 1201 (2008).
2. K. Ishida, Y. Nakai, and H. Hosono, J. Phys. Soc. Jpn. **78**, 062001 (2009).
3. D. C. Johnston, Adv. Phys. **59**, 803 (2010).
4. P. J. Hirschfeld, M. M. Korshunov, and I. I. Mazin, Rep. Prog. Phys. **74**, 124508 (2011).
5. G. R. Stewart, Rev. Mod. Phys. **83**, 1589 (2011).
6. A. A. Kordyuk, Low Temp. Phys. **38**, 888 (2012).
7. Y. Mizuguchi and Y. Takano, J. Phys. Soc. Jpn. **79**, 102001 (2010).
8. M. Sadovskii, E. Kuchinskii, and I. Nekrasov, J. Magn. Magn. Mater. **324**, 3481 (2012).
9. I. A. Nekrasov and M. V. Sadovskii, JETP Lett. **99**, 598 (2014).
10. J. Guo, S. Jin, G. Wang, S. Wang, K. Zhu, T. Zhou, M. He, and X. Chen, Phys. Rev. B **82**, 180520 (2010).
11. Y. J. Yan, M. Zhang, A. F. Wang, J. J. Ying, Z. Y. Li, W. Qin, X. G. Luo, J. Q. Li, J. p. Hu, and X. H. Chen, Sci. Rep. **2** (2012). doi 10.1038/srep00212
12. A. Krzton-Maziopa, V. Svitlyk, E. Pomjakushina, R. Puzniak, and K. Conder, J. Phys.: Condens. Matter **28**, 293002 (2016).
13. T. Hatakeda, T. Noji, T. Kawamata, M. Kato, and Y. Koike, J. Phys. Soc. Jpn. **82**, 123705 (2013).
14. M. Burrard-Lucas, D. G. Free, S. J. Sedlmaier, J. D. Wright, S. J. Cassidy, Y. Hara, A. J. Corkett, T. Lancaster, P. J. Baker, S. J. Blundell, and S. J. Clarke, Nat. Mater. **12**, 15 (2013).
15. X. F. Lu, N. Z. Wang, H. Wu, Y. P. Wu, D. Zhao, X. Z. Zeng, X. G. Luo, T. Wu, W. Bao, G. H. Zhang, F. Q. Huang, Q. Z. Huang, and X. H. Chen, Nat. Mater. **14**, 325 (2014).
16. U. Pachmayr, F. Nitsche, H. Luetkens, S. Kamusella, F. Brückner, R. Sarkar, H.-H. Klauss, and D. Johrendt, Angew. Chem. Int. Ed. **54**, 293 (2015).
17. Q.-Y. Wang, Z. Li, W.-H. Zhang, Z.-C. Zhang, J.-S. Zhang, W. Li, H. Ding, Y.-B. Ou, P. Deng, K. Chang, J. Wen, C.-L. Song, K. He, J.-F. Jia, S.-H. Ji, et al., Chin. Phys. Lett. **29**, 037402 (2012).
18. J.-F. Ge, Z.-L. Liu, C. Liu, C.-L. Gao, D. Qian, Q.-K. Xue, Y. Liu, and J.-F. Jia, Nat. Mater. **14**, 285 (2014).
19. Y. Miyata, K. Nakayama, K. Sugawara, T. Sato, and T. Takahashi, Nat. Mater. **14**, 775 (2015).
20. G. Zhou, D. Zhang, C. Liu, C. Tang, X. Wang, Z. Li, C. Song, S. Ji, K. He, L. Wang, X. Ma, and Q.-K. Xue, Appl. Phys. Lett. **108**, 202603 (2016).
21. R. Peng, H. C. Xu, S. Y. Tan, H. Y. Cao, M. Xia, X. P. Shen, Z. C. Huang, C. Wen, Q. Song, T. Zhang, B. P. Xie, X. G. Gong, and D. L. Feng, Nat. Comm. **5**, 5044 (2014).
22. H. Ding, Y.-F. Lv, K. Zhao, W.-L. Wang, L. Wang, C.-L. Song, X. Chen, X.-C. Ma, and Q.-K. Xue, Phys. Rev. Lett. **117**, 067001 (2016).
23. C.-L. Song, Y.-L. Wang, Y.-P. Jiang, Z. Li, L. Wang, K. He, X. Chen, X.-C. Ma, and Q.-K. Xue, Phys. Rev. B **84** (2011). doi 10.1103/PhysRevB.84.020503
24. X. Liu, L. Zhao, S. He, J. He, D. Liu, D. Mou, B. Shen, Y. Hu, J. Huang, and X. J. Zhou, J. Phys.: Condens. Matter **27**, 183201 (2015).
25. M. V. Sadovskii, Phys. Usp. **59**, 947 (2016).
26. E. Z. Kuchinskii and M. V. Sadovskii, JETP Lett. **91**, 660 (2010).
27. S. L. Skornyakov, A. V. Efremov, N. A. Skorikov, M. A. Korotin, Y. A. Izyumov, V. I. Anisimov, A. V. Kozhevnikov, and D. Vollhardt, Phys. Rev. B **80** (2009). doi 10.1103/PhysRevB.80.092501
28. I. A. Nekrasov, N. S. Pavlov, and M. V. Sadovskii, JETP Lett. **102**, 26 (2015).
29. I. A. Nekrasov and M. V. Sadovskii, JETP Lett. **93**, 166 (2011).
30. I. Shein and A. Ivanovskii, Phys. Lett. A **375**, 1028 (2011).
31. L. Zhao, D. Mou, S. Liu, X. Jia, J. He, Y. Peng, L. Yu, X. Liu, G. Liu, S. He, X. Dong, J. Zhang, J. B. He, D. M. Wang, G. F. Chen, et al., Phys. Rev. B **83** (2011). doi 10.1103/PhysRevB.83.140508

32. I. A. Nekrasov, N. S. Pavlov, and M. V. Sadovskii, JETP Lett. **97**, 15 (2013).
33. I. A. Nekrasov, N. S. Pavlov, and M. V. Sadovskii, J. Exp. Theor. Phys. **117**, 926 (2013).
34. I. A. Nekrasov, N. S. Pavlov, and M. V. Sadovskii, JETP Lett. **105**, 370 (2017).
35. M. Yi, D. H. Lu, R. Yu, S. C. Riggs, J.-H. Chu, B. Lv, Z. K. Liu, M. Lu, Y.-T. Cui, M. Hashimoto, S.-K. Mo, Z. Hussain, C. W. Chu, I. R. Fisher, Q. Si, and Z.-X. Shen, Phys. Rev. Lett. **110** (2013). doi 10.1103/PhysRevLett.110.067003
36. X. H. Niu, S. D. Chen, J. Jiang, Z. R. Ye, T. L. Yu, D. F. Xu, M. Xu, Y. Feng, Y. J. Yan, B. P. Xie, J. Zhao, D. C. Gu, L. L. Sun, Q. Mao, H. Wang, et al., Phys. Rev. B **93** (2016). doi 10.1103/PhysRevB.93.054516
37. I. A. Nekrasov, N. S. Pavlov, M. V. Sadovskii, and A. A. Slobodchikov, Low Temp. Phys. **42**, 891 (2016).
38. A. Subedi, L. Zhang, D. J. Singh, and M. H. Du, Phys. Rev. B **78** (2008). doi 10.1103/Phys-RevB.78.134514
39. F. Zheng, Z. Wang, W. Kang, and P. Zhang, Sci. Rep. **3**, 2213 (2013).
40. P. Blaha, K. Schwarz, G. K. H. Madsen, D. Kvasnicka, and J. Luitz, *An Augmented Plane Wave + Local Orbitals Program for Calculating Crystal Properties wIEN2k 16.1, Release12/12/2016* (Vienna Univ. Technol., Inst. Mater. Chem., Vienna, Austria, 2016).
41. J. Kune, R. Arita, P. Wissgott, A. Toschi, H. Ikeda, and K. Held, Comput. Phys. Comm. **18181**, 1888 (2010).
42. A. A. Mosto, J. R. Yates, Y.-S. Lee, I. Souza, D. Vanderbilt, and N. Marzari, Comput. Phys. Comm. **178**, 685 (2008).
43. P. Werner, A. Comanac, L. de'Medici, M. Troyer, and A. J. Millis, Phys. Rev. Lett. **97**, 076405 (2006).
44. K. Haule, Phys. Rev. B **75**, 155113 (2007).
45. E. Gull, A. J. Millis, A. I. Lichtenstein, A. N. Rubtsov, M. Troyer, and P. Werner, Rev. Mod. Phys. **83**, 349 (2011).
46. O. Parcollet, M. Ferrero, T. Ayral, H. Hafermann, I. Krivenko, L. Messio, and P. Seth, Comput. Phys. Commun. **196**, 398 (2015). http://ipht.cea.fr/triqs.
47. I. A. Nekrasov, N. S. Pavlov, and M. V. Sadovskii, J. Exp. Theor. Phys. **116**, 620 (2013).
48. H. J. Vidberg and J. W. Serene, J. Low Temp. Phys. **29**, 179 (1977).
49. M. Jarrell and J. Gubernatis, Phys. Rep. **269**, 133 (1996).
50. D. Liu, W. Zhang, D. Mou, J. He, Y.-B. Ou, Q.-Y. Wang, Z. Li, L. Wang, L. Zhao, S. He, Y. Peng, X. Liu, C. Chen, L. Yu, G. Liu, X. Dong, J. Zhang, C. Chen, Z. Xu, J. Hu, X. Chen, X. Ma, Q. Xue, and X. Zhou, Nat. Comm. **3**, 931 (2012).
51. J. J. Lee, F. T. Schmitt, R. G. Moore, S. Johnston, Y.-T. Cui, W. Li, M. Yi, Z. K. Liu, M. Hashimoto, Y. Zhang, D. H. Lu, T. P. Devereaux, D.-H. Lee, and Z.-X. Shen, Nature (London, U.K.) **515**, 245 (2014).
52. L. Zhao, A. Liang, D. Yuan, Y. Hu, D. Liu, J. Huang, S. He, B. Shen, Y. Xu, X. Liu, L. Yu, G. Liu, H. Zhou, Y. Huang, X. Dong, F. Zhou, K. Liu, Z. Lu, Z. Zhao, C. Chen, Z. Xu, and X. J. Zhou, Nat. Comm. **7**, 10608 (2016).
53. H. Fu, K. V. Reich, and B. I. Shklovskii, J. Exp. Theor. Phys. **122**, 456 (2016).
54. Y. Zhou and A. J. Millis, Phys. Rev. B **93**, 224506 (2016).
55. M. X. Chen, Z. Ge, Y. Y. Li, D. F. Agterberg, L. Li, and M. Weinert, Phys. Rev. B **94**, 245139 (2016).
56. J. J. Lee, F. T. Schmitt, R. G. Moore, S. Johnston, Y.-T. Cui, W. Li, M. Yi, Z. K. Liu, M. Hashimoto, Y. Zhang, D. H. Lu, T. P. Devereaux, D.-H. Lee, and Z.-X. Shen, Nature (London, U.K.) **515**, 245 (2014).
57. L. P. Gor'kov, Phys. Rev. B **93**, 060507 (2016).
58. L. P. Gor'kov, Phys. Rev. B **93**, 054517 (2016).
59. L. Rademaker, Y. Wang, T. Berlijn, and S. Johnston, New J. Phys. **18**, 022001 (2016).
60. Y. Wang, K. Nakatsukasa, L. Rademaker, T. Berlijn, and S. Johnston, Supercond. Sci. Technol. **29**, 054009 (2016).
61. M. Sunagawa, K. Terashima, T. Hamada, H. Fujiwara, T. Fukura, A. Takeda, M. Tanaka, H. Takeya, Y. Takano, M. Arita, K. Shimada, H. Namatame, M. Taniguchi, K. Suzuki, H. Usui, K. Kuroki, T. Wakita, Y. Muraoka, and T. Yokoya, J. Phys. Soc. Jpn. **85**, 073704 (2016).
62. M. D. Watson, T. K. Kim, A. A. Haghighirad, N. R. Davies, A. McCollam, A. Narayanan, S. F. Blake, Y. L. Chen, S. Ghannadzadeh, A. J. Schoeld, M. Hoesch, C. Meingast, T. Wolf, and A. I. Coldea, Phys. Rev. B **91**, 155106 (2015).
63. L. de Medici, G. Giovannetti, and M. Capone, Phys. Rev. Lett. **112**, 177001 (2014).
64. Z. P. Yin, K. Haule, and G. Kotliar, Nat. Mater. **10**, 932 (2011).
65. M. L. Kulic and O. V. Dolgov, New J. Phys. **19**, 013020 (2017).
66. O. V. Danylenko, O. V. Dolgov, M. L. Kulić, and V. Oudovenko, Eur. Phys. J. B **9**, 201 (1999).
67. M. L. Kulić, AIP Conf. Proc. **715**, 75 (2004).
68. P. B. Allen, Phys. Rev. B **6**, 2577 (1972).
69. Y. Wang, A. Linscheid, T. Berlijn, and S. Johnston, Phys. Rev. B **93**, 134513 (2016).
70. Y. Zhou and A. J. Millis, arXiv:1703.04021 (2017).